Macromolecules
ARTICLE

Macromolecules **2010**, *43*, 6495–6504 **6495**
DOI: 10.1021/ma1006733

Directed Assembly of a Cylinder-Forming Diblock Copolymer: Topographic and Chemical Patterns

François A. Detcheverry, Paul F. Nealey, and Juan J. de Pablo*

Department of Chemical and Biological Engineering, University of Wisconsin—Madison, Madison, Wisconsin, 53706-1691

Received March 29, 2010; Revised Manuscript Received June 10, 2010

ABSTRACT: Using simulations of a coarse-grained model, we examine the ability of topographic and chemical patterns to direct the self-assembly of thin films of copolymers into a defect-free array of vertical cylinders. The topographic pattern is a trench where the diblock is confined, whereas the chemical pattern consists of spots that interact preferentially with the minority block. The self-assembly process is described with Monte Carlo simulations of the standard model of block copolymers. While fully three-dimensional, the simulated systems can include over a hundred domains. By analyzing top views and cross sections of thin films, it is possible to determine the degree of ordering and the properties of individual domains. First, the influence of confinement on ordering perfection is examined. By focusing on the influence of trench width and sidewall selectivity, one can identify conditions that yield defect-free arrays with a high reliability and for which domains exhibit a high degree of uniformity across the trench. Second, we consider chemical patterns. While patterns matching the block copolymer morphology and characteristic dimensions yield defect-free self-assembly, we study the tolerance of directed self-assembly against deviations from this optimal case. We first explore the effect of a mismatch between the spacing of the pattern and the diblock characteristic dimensions, and then we examine the interpolation of domains on an incomplete pattern, where half of the rows are missing. By introducing placement error in the position of the spots, we assess to what extent the diblock can rectify the noise of a substrate pattern. The results of simulations are discussed in the context of a variety of experimental observations.

I. Introduction

Directed self-assembly of block copolymers into ordered morphologies[1] offers a promising route toward inexpensive fabrication of nanostructures. Some of the features that make copolymers attractive for nanofabrication include the range of length scales that are accessible, the variety of morphologies that can arise,[2] and the ability to tailor the properties of the self-assembled system by changing the block copolymer, the thermodynamic parameters, or the processing conditions. With current lithographic methods reaching their limit, one important application of block copolymers will likely involve the production of next-generation, ultrahigh density memory storage devices, where copolymers can enable facile fabrication of bit-patterned media. The target template in this context consists of a large number (10^{12}) of domains, each a few nanometers in size, arranged in a periodic array, with no defects. The challenge associated with the use of block copolymers is that the periodicity of spontaneously self-assembled structures is local rather than global.[3] The short-range order gives way to defects that disrupt the periodicity beyond a correlation length $\xi \sim 10-100\, d_0$, where d_0 is the block copolymer natural spacing. As seen both in experiments[4,5] and in simulations,[6] the grain size increases with time as $\xi \sim t^{\eta}$, with η in the range 0.2−0.25. As a result of this slow coarsening dynamics, ordered regions rarely extend beyond μm length scales, even after weeks of annealing. In contrast, defect-free arrangements over macroscopic areas are required for many electronic devices, and for the self-assembly process to be integrated into industrial production it must occur on faster time scales. Besides issues related to equilibration, an additional difficulty is that thin films of block copolymers are not expected to reach perfect ordering even at equilibrium. In a two-dimensional system, the positional order is quasi-long-range at best, i.e., it decays as a power law of the distance, because of a finite concentration of thermally activated defects.[7]

Several approaches have been proposed to address the challenge of long-range order.[3,8−10] One class of methods involves the use of nonequilibrium processes or external fields; examples include the use of flow or electric fields, controlled evaporation of solvent, or directional solidification. A second strategy relies on substrates with topographic or chemical patterns. By tailoring the boundary conditions, the self-assembly can be directed toward the intended structure. It is this second strategy that is examined in this work.

The use of a topographic pattern, generically referred to as "graphoepitaxy", encompasses a variety of situations. Early work introduced a substrate patterned with shallow steps, several micrometers apart from each other.[11] In that case complete alignment of spherical domains is favored in the vicinity of the steps, and the order is found to extend to other rows away from the wall. When the distance between the two vertical walls is comparable to the natural spacing of the copolymer, the effect of commensurability becomes important. Confinement in a trench, which is also referred to as channel, groove or trough, has attracted the most attention and has now been studied for all the canonical morphologies, including lamellae,[12,13] horizontal or vertical cylinders,[14,15] and spheres.[8,11,16] Variations on this one-dimensional confinement include tapered trenches,[17] modulation

*Corresponding author.

Published on Web 07/07/2010

of the trench width,[18] roughness in the line edge,[19] and V-shaped grooves.[20] More recently, the effects of less confining topographic patterns have also been considered. One study has introduced a sparse array of nanoscale posts that act as surrogates for the domains,[21] and another has shown that a substrate with a sawtoothed topography can ensure the lateral ordering of vertical cylinders laying above it.[22]

Chemical patterns, produced by a local change in the chemical functionality of the substrate, have also been shown to lead to defect-free assembly over arbitrarily large areas.[23,24] Of particular interest has been the demonstration that "incomplete" or "sparse" patterns can be used to direct the assembly of block copolymers.[25−27] In such a technique, referred to as "density multiplication" or "pattern interpolation", the block copolymer adds information into the patterning process beyond that encoded in the substrate pattern. In that context, the block copolymer also serves to rectify imperfections in the size and position of patterned spots, thereby leading to what could be called a self-correcting patterning technique. Interpolation and rectification effects are therefore two particularly appealing advantages of chemical patterning strategies. However, it is still necessary to pattern spots having dimensions comparable to those of the polymer domains. This requirement should be contrasted with graphoepitaxy where, ideally, the topographic pattern could have characteristic dimensions that are larger than those of the copolymer domains, thereby facilitating fabrication.

Many factors come into play in deciding which types of patterns are most suitable for production of ultradense, macroscopic, defect-free arrays. The focus of this work is the quality of the self-assembled nanostructures, including the positional order of domains and their uniformity. As alluded to earlier, a growing body of experimental work has sought to identify the respective merits of topographic and chemical patterns. In comparison, progress on the theoretical and computational side has been limited. A major obstacle has been the scale of the systems that must be considered. The concentration of defects observed in experiments is in the range between 10^{-2} to10^{-4}, and many intended applications require an ultralow defect density.[25,27] In the absence of theoretical approaches for defect formation, predicting defect concentrations will likely require simulations with a large number of domains. Note that current numerical approaches are routinely used to determine the block copolymer morphology, but identifying the optimal conditions for defect-free assembly represents a different, and genuine challenge.

Given the scale of the problem, a coarse-grained description of the copolymer is warranted. Phenomenological models that rely on a Ginzburg−Landau free energy with nonlocal interactions can generate efficient simulations of ordering in a diblock copolymer.[28,29] However, since the notion of a polymer chain is not explicit in such approaches, extensions to multicomponent systems such as copolymer or copolymer-homopolymer blends appear difficult. This is a significant limitation because it is increasingly clear that blends are very relevant to block copolymer lithography; they can enable formation of nonbulk, technologically important morphologies, including square arrays of cylinders[30] or nonregular, deviced-oriented geometries[31] that can not be obtained with pure copolymers.

Self-consistent field theory (SCFT) provides an alternative approach for study of the effects of patterns on self-assembly.[30,32,33] The underlying description of the molecules is the standard model of block copolymers[34] which, unlike more phenomenological approaches, takes into account the polymeric nature of the system in an explicit manner. A recent study[33] considered the effects of confining a diblock copolymer in a hexagonal cavity and identified the "commensurability window", i.e., the range in cavity size that leads to a defect-free array of domains. While the cavity was large enough to accommodate around 60 domains, the system was two-dimensional, partly because describing such large systems with standard computational capabilities is facilitated by postulating invariance in the direction normal to the substrate. This two-dimensional assumption precludes studies of the interplay between the block copolymer characteristics, the pattern properties, the film thickness and, more importantly, it does not hold in many situations of technological interest, such as bit patterned media fabrication. In the presence of chemically patterned substrates, invariance across the film is the exception rather than the rule, in particular for blend systems where one can expect inhomogeneous distribution of homopolymer across the film.[24] Technological relevance requires a fully three-dimensional description of the copolymer films.

The goal of this work is to analyze the ability of topographic and chemical patterns to yield dense, defect-free arrays of copolymer domains. We use theoretically informed Monte Carlo simulations of the standard model of block copolymers, a method that relies on the field-based Hamiltonian underlying traditional SCFT calculations, but that permits a particle-based representation which is amenable to Monte Carlo simulations. Compared to our previous works using this approach,[25,35−37] the present study differs in two respects. First, instead of focusing on the type of self-assembled morphology, we address the positional order of domains, whose number must be significant. Our method is sufficiently efficient to simulate fully three-dimensional systems, each containing over a hundred domains. Second, we describe, albeit in an approximate manner, the dynamics of self-assembly. Instead of resorting to the global (but unphysical) Monte Carlo moves that are useful to reach the equilibrium morphology, the Monte Carlo moves employed here are local only, and it is assumed that the simulation generates a pseudodynamics for the self-assembly process. This approach is closely related to single-chain in mean field simulations,[38] and is comparable to other methods that operate at the same mesoscopic level, such as dynamic density functional theory.[39,40]

The test system studied here has been considered in detail in experimental studies[15,25,41] and involves a cylinder-forming block copolymer that should self-assemble into vertical domains. The topographic pattern is a trench of constant width, the chemical pattern is a hexagonal array of spots that interact selectively with the minority block. When comparing graphoepitaxy and chemical patterns, we follow somewhat opposite approaches. For the former, we seek to determine whether confinement in a trench can lead to the perfection of ordering that is required for applications. By investigating the influence of the trench's width on the resulting morphology, we progressively narrow down the system's parameters to one set of optimal conditions, for which we characterize the properties of domains. Chemical patterns, on the other hand, are known to yield defect-free structures when the pattern matches the block copolymer morphology and natural dimensions. In experiments, however, those patterns include noise or imperfections. The aim of our work is then to gauge the robustness of the self-assembly approach against deviations from optimal, perfectly commensurate conditions. Three kinds of deviations are considered here. First, we vary the pattern spacing and assess the tolerance against a mismatch in dimensions. Second, we change the number of spots and explore the possibility of interpolation. Third, we add noise to the spot positions and characterize the rectification effect. Before examining self-assembly on the patterns, we briefly describe the model, the test system and the analysis method.

II. Model

This section summarizes the model and method employed here; the reader is referred to ref 36 for an overview and to ref 35 for a more detailed account. Our starting point is the standard

model for a block copolymer melt,[34] which assumes Gaussian chains and describes nonbonded interactions with a functional of the local density. For a system of n AB block copolymer chains, each discretized into N beads, in a volume V at temperature T, the Hamiltonian is given by

$$\frac{\mathscr{H}}{k_B T} = \frac{3}{2}\sum_{i=1}^{n}\sum_{s=1}^{N-1}\frac{N-1}{{R_e}^2}[\mathbf{r}_i(s+1)-\mathbf{r}_i(s)]^2 + \sqrt{\bar{N}}\int_V \frac{\mathrm{d}\mathbf{r}}{{R_e}^3}\left[\chi N\phi_A\phi_B + \frac{\kappa N}{2}(1-\phi_A-\phi_B)^2\right] \quad (1)$$

Here, k_B is the Boltzmann constant, ${R_e}^2$ is the mean squared end-to-end distance for an ideal chain, $\mathbf{r}_i$(s) is the position of the s^{th} bead in the i^{th} chain, and $\bar{N}^{1/2} = \rho_o {R_e}^3/N$ where ρ_0 is the bead density, is the interdigitation number. The strength of repulsion between unlike blocks is controlled by χN, and the compressibility of the melt is fixed by κN. The local densities $\phi_{K=A,B}$ are computed from the positions of the beads by counting the number of beads in the cells of a regular grid with grid spacing ΔL.

To model a thin film of block copolymer, the chains are confined between two hard walls.[57] The block-surface interaction is represented at a coarse-grained level by a short-range bead-surface potential U_S of the form

$$\frac{U_S(\mathbf{r},K)}{k_B T} = -\frac{\Lambda_S^K}{d_S/R_e}\exp\left[-\frac{z^2}{2{d_S}^2}\right] \quad (2)$$

where $\mathbf{r}$ is the bead's position, $K = A, B$ its type, z is the distance from the surface, and d_S is the interaction range. Λ_S^K determines the strength and sign of interaction, it is constant for a homogeneous surface and depends on position for a patterned surface.

III. Results

A. Preliminary. *1. Thin Film Properties.* We consider an asymmetric diblock copolymer discretized into $N = N_A + N_B = 9 + 23 = 32$ beads, which corresponds to a volume fraction of 0.28 for the minority block. In line with the discussion of ref 42, the compressibility parameter is fixed to $\kappa N = 50$. The interdigitation number is $\sqrt{\bar{N}} = 128$ and $\chi N = 25$. This set of parameters is representative of experimental systems used in block copolymer lithography.[23−25] A typical end-to-end distance would be $R_e = 30$ nm, a value that will be used throughout this work to convert simulation length scales to real units. As in previous works,[35,43] the grid spacing $\Delta L = 0.15 R_e$ is chosen so that each bead interacts with a large number of other beads. The largest systems considered here include more than 10^5 chains, i.e., several million beads.

While the bulk diblock adopts a cylindrical morphology, confinement in a thin film and preferential wetting at the surface can change the orientation of domains and the type of morphology. Those effects have been studied with a variety of approaches, including strong segregation theory,[44] dynamic density functional theory,[45] Monte Carlo simulations of a lattice model,[46] and SCFT.[47,48] Figure 1 shows the various morphologies found in our simulations, when the top and bottom surfaces are both neutral ($\Lambda N = 0$). Since the size of the simulation box is finite and is not exactly commensurate with the natural spacing of the ordered morphology, it could induce artifacts and spuriously influence the morphology observed. We use rather large systems, with minimum dimensions $L_x \simeq 10.5\ R_e$ and $L_y \simeq 12\ R_e$, that can accommodate more than 40 vertical cylinders; finite-size effects are expected to be small for such system sizes.[58] Because only the equilibrium morphology is of interest here, global Monte Carlo moves are employed, including reptation moves, translation of a whole chain and switching the identity of the blocks. All observed morphologies have cylindrical domains. As found in previous works, the orientation of cylinders is highly dependent on the film thickness. Indeed, even a perfectly neutral wall introduces several effects.[49] The enrichment of chain ends near the surface induces an effective attraction between the shorter block and the wall. On the other hand, the drop in density at the wall reduces the enthalpic penalty of an A−B interface, which favors locating the interfaces at the wall.

L_z/R_e	Case
0.5-1	a
1.125-1.75	b
2-2.2	a
2.25	c
2.5-3.75	d
4-4.5	e

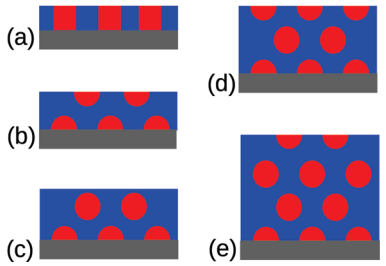

Figure 1. Morphologies observed in a thin film confined between two neutral surfaces as a function of film thickness. A schematic representation of the system is shown on the right for each case.

The vertically oriented cylinders that form the target morphology of this study are obtained for $L_z = (0.5-1)R_e$ and $L_z = (2-2.2)R_e$. Because a high aspect ratio is important for fabrication processes, the film thickness is set to $L_z = 2.2R_e$. To compute the natural spacing d_0 of the cylinders in the thin film, we simply use a large system, which, after equilibration, exhibits a defect-free array of 236 cylinders. The distribution of distance between nearest-neighbor cylinders is approximately Gaussian, with a standard deviation $0.12R_e$, and an average value $d_0 = 1.74R_e$. Note that a bottom substrate with a weak attraction for the majority component would favor the perpendicular orientation of domains. We have chosen a neutral substrate since it offers favorable conditions for interpolation of domains.

2. Pseudodynamics. Monte Carlo simulations can yield a qualitative description of the dynamics, provided the moves employed are not too different from the actual motion of the chain (see ref 38 for an example in the related context of single-chain in mean field simulations). At least two simple pseudodynamics for the polymer chains can be considered. Restricting moves to random displacements of individual beads leads to a Rouse dynamics for the chains. On the other hand, when the topological constraints imposed by the surroundings chains are important, the slithering-snake move can be used to mimic the reptating motion of the molecules (see ref 50, however). Those two pseudodynamics would apply in the limit of low or high molecular weight, when the entanglements are negligible or prevailing, respectively. The system considered in this work falls in an intermediate regime. Consider, for example, a PS−PMMA copolymer, which is commonly used in experiments, with molecular weight 100 kg·mol^{-1}. Given that the entanglement molecular weights of PS and PMMA are 13 and 10 kg·mol^{-1} respectively,[51] entanglements are not negligible.

We chose a pseudodynamics that combines single displacement and slithering-snake (reptation) moves, with respective proportion 80% and 20%. This choice is rather arbitrary, the resulting dynamics is not expected to be realistic at

the single-chain level, and it entirely neglects hydrodynamic interactions (which are unlikely to be important in the dense polymer melts considered here). However, it captures the diffusive relaxation kinetics of composition fluctuations, and we assume it provides a reasonable description of the dynamics at a collective level, i.e., at the level of domains.[59] In the single displacement move, the maximum displacement is set so that the acceptance ratio is 40%.[60] In the slithering-snake move, the number of beads moved from one chain end to the other is randomly chosen in the range [1,3] which gives an acceptance ratio of around 50% in the ordered phase. With the convention that a slithering-snake move displaces an average number of four beads, each particle experiences on average one trial move at each Monte Carlo step (MCS).

An estimate of the simulation time scale is provided by computing the diffusion coefficient D according to

$$\lim_{t\to\infty} \langle \mathbf{r}_{ccm}{}^2(t)\rangle = 6Dt \tag{3}$$

where $\langle\rangle$ denotes a thermodynamic average, and $\mathbf{r}_{ccm}(t)$ is the displacement vector of the chain center of mass after a time t expressed in MCS. For a homopolymer, we find $D = 3.5\times10^{-3}\ R_e{}^2\cdot\mathrm{MCS}^{-1}$ in the bulk and $D = 2.2\times10^{-3}\ R_e{}^2\cdot\mathrm{MCS}^{-1}$ in a film of thickness $L_z = 2.2R_e$. The longest simulations presented below reach 2×10^5 MCS, during which a homopolymer chain can diffuse over a distance $50R_e$. In the diblock system, diffusion is suppressed, but the time range simulated is still large and, indeed, all systems reach a stable configuration. The initial condition for the pseudodynamic simulations is a disordered phase at $\chi N = 0$, which is then quenched to $\chi N = 25$.

3. Analysis. Snapshots of the system are periodically recorded to follow the self-assembly process and investigate the dimensions and positional order of the domains. We use top views because they are accessible in experiments, whereas three-dimensional visualization, from cross sections for instance, is much more difficult to achieve. For a thin layer at the top of the film ($2 < z/R_e < 2.2$), a two-dimensional map of the local composition $\phi = \phi_A - \phi_B$ is computed using a regular grid with lattice spacing $0.05\ R_e$. To obtain sufficient resolution, ϕ is averaged over 200 MCS. Individual domains are identified by performing a cluster analysis for sites where $\phi > 0$.[61] The effective "area" of a cluster is defined as $A = \sum_i \phi_i$, where the sum runs over all cluster sites. After discarding clusters of negligible area, each remaining cluster corresponds to the top section of a cylindrical domain. A cluster is then characterized by its radius $R = (A/\pi)^{1/2}$, and the position of its center of mass $\mathbf{r}_{cm} = 1/A\sum_i \phi_i \mathbf{r}_i$, where $\mathbf{r}_i$ is the position of site i. The gyration tensor $G_{\alpha\beta} = 1/A\sum_i \phi_i r_{i,\alpha} r_{i,\beta}$ where $\alpha,\beta \in \{x, y\}$, is also computed, as well as its two eigenvalues $\lambda_+{}^2 > \lambda_-{}^2$. The shape of a domain is characterized by the ratio between the long and short axes $\gamma = \lambda_+/\lambda_- - 1$ and the eccentricity $\varepsilon = (1-(\lambda_-/\lambda_+)^2)^{1/2}$. Finally, the number of neighboring domains and the distance to them was computed from a Delaunay triangulation. Occasionally, two neighboring cylinders are seen to merge at their top to form a bridge that connects them into a single cluster. Those paired domains can easily be identified from their large radius of gyration and the bridge is then broken before performing the analysis.[62] The analysis of top views is sufficient to characterize the system self-assembled on a neutral substrate because a cylindrical domain and its top section have the same average position. Such is not the case for patterned substrates, and a fully three-dimensional characterization is then implemented.

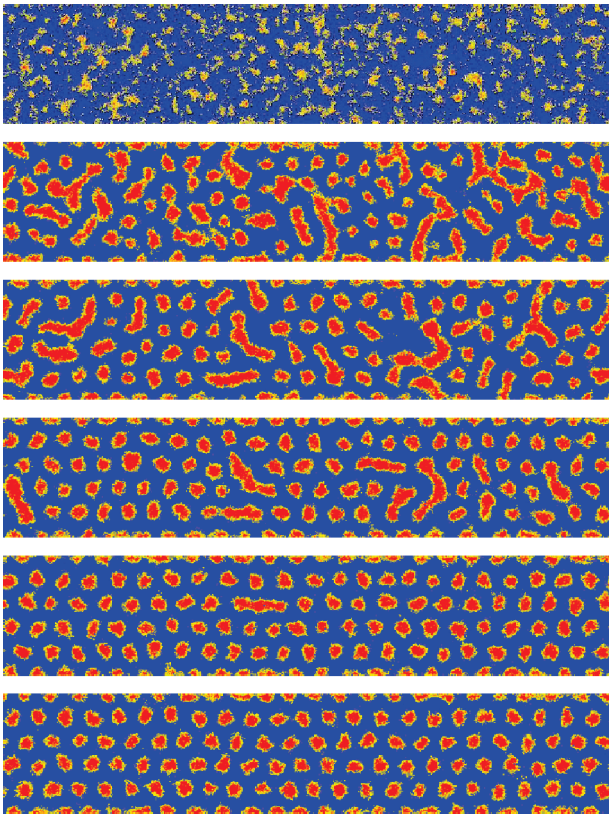

Figure 2. Dynamics of self-assembly in a trench. Top views of the system are taken after 200, 600, 4000, 10000, 40000, and 80000 MCS (from top to bottom). The color map indicates the local composition ϕ, with A-rich areas in red ($\phi \simeq 1$), B-rich areas in blue ($\phi \simeq -1$) and equal density of A and B in yellow ($\phi \simeq 0$). In the final state, each domain corresponds to a vertically oriented cylinder. The trench dimensions are $L_x = 40R_e$, $L_y = 7.93R_e$, and $L_z = 2.2R_e$, the sidewalls are neutral.

B. Graphoepitaxy. In this section we examine how confinement in a trench affects the quality of the self-assembled structure; seeking to identify optimal conditions, we focus on the influence of trench width and sidewall selectivity. The system considered here consists of a trench of width L_y and length L_x, with periodic boundary conditions in the x direction. The bottom substrate and top surface are neutral ($\Lambda^A N = \Lambda^B N = 0$), but the sidewalls are either neutral, B-selective, or A-selective. In the latter case, the surface potential has a range of $0.15R_e$ and strength $\Lambda^A N = -\Lambda^B N = 0.5$, i.e., the sidewall exerts an attraction on the A beads and a repulsion on the B beads of equal magnitude. Whereas neutral sidewalls result in the formation of half-cylinders along the trench edges, A-selective sidewalls are entirely covered by a preferential wetting layer of A beads. In both cases, the "edge rows", i.e., the rows immediately adjacent to the trench edge, consist of individual cylindrical domains. In contrast, for the case of the B-selective sidewalls, neighboring domains sometimes merge together. Since those larger domains would be detrimental for the intended applications, only neutral and A-selective sidewalls are considered in what follows. For brevity, the two systems are referred to as the neutral trench and selective trench, respectively.

Figure 2 illustrates the various stages of the self-assembly process. First, a rapid microphase separation gives rise to domains having a variety of shapes and sizes. While some domains are already vertical, long, horizontal domains that are roughly semicylindrical in shape are also seen at the top of the film; they subsequently break up to form several vertical cylinders. As a consequence, the number of domains

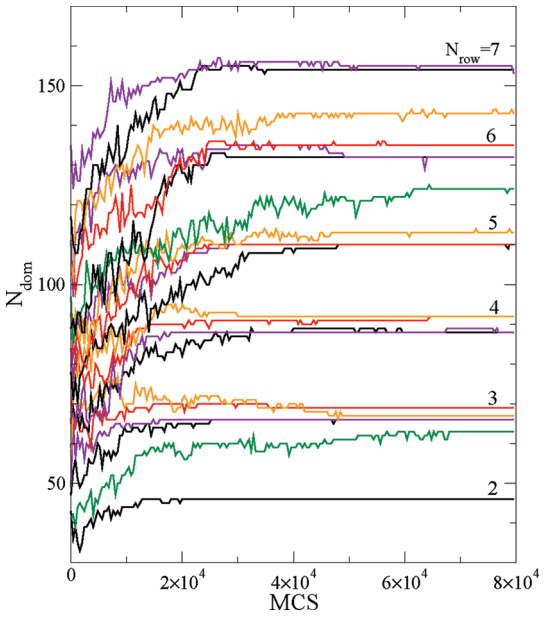

Figure 3. Number of domains in the trench, as seen from a top view. Each of the 21 curves corresponds to a trench width L_y ranging from $5.4R_e$ to $12.6R_e$, from bottom to top. The number of rows is indicated on the right side. The sidewalls are neutral.

seen in the top view generally increases with time. The hexagonal order in the domain position appears simultaneously in different parts of the trench, but the merging of those locally ordered regions into the final self-assembled structure is a slow process: compare, for instance, the last two snapshots of Figure 2 taken at 40000 MCS and after the system evolved for an additional 40000 MCS. Such slow coarsening kinetics can be expected when only a few defects are left and the forces driving the evolution of the system are weak.

To study commensurability effects, the trench width was varied systematically, from $L_y = 5.4R_e$ to $12.6R_e$ in regular increments of $0.36R_e$, while keeping $L_x = 40R_e$. The narrowest trench contains two rows and 46 cylinders, the largest trench contains seven rows and more than 150 cylinders. The number of domains N_{dom} is plotted in Figure 3 as a function of time; it increases until it reaches a plateau that corresponds to a stable state. Perhaps surprisingly, the time necessary to reach this final configuration does not systematically increase with the number of rows N_{row}. Rather, for a given N_{row}, there is an optimal width that leads to the fastest ordering, in 30000 MCS or less. Trench widths that are half way between those optimal values lead to the longest equilibration times. After 10^5 MCS, a stable self-assembled state is reached in all cases. We can not ascertain that this configuration corresponds to equilibrium or that it would remain unchanged over the course of much longer simulations; however, it is stable for the pseudodynamics considered in this work.

The final configurations can be classified into three types: (i) defect-free array (ii) individual dislocation, when cylinders are missing in one or several rows (iii) "coexistence", when the trench contains two well-ordered regions with n and $n + 1$ rows.[63] Each case is illustrated in Figure 4. Several experimental studies[15,16,18,52] have reported on the number or rows as a function of trench width. Our results are shown in Figure 5 which also indicates the type of arrangement. Defective structures are more likely to be found at the edges of each step, as expected. Defect-free arrangements, on the other hand, are more common in the narrowest trenches. For instance, when $N_{row} = 3$, four trench widths, out of the five

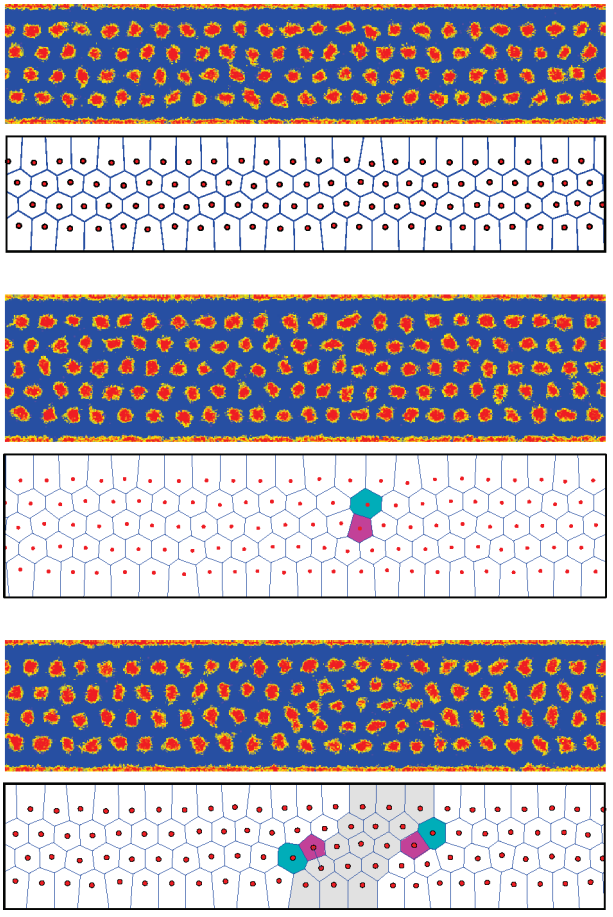

Figure 4. Type of domain arrangement found in the self-assembled system: (top) defect-free configuration; (middle) individual dislocation, where one domain is missing in each of the two upper rows; (bottom) coexistence of four rows and five rows (shaded area). The color scheme for the snapshots is similar to that of Figure 2. In the Voronoi diagrams, each dot corresponds to the center of a domain top section and a line connecting two dots indicates a bridge between domains (see text). Cells are colored when the number of neighbors is five (magenta) or seven (cyan). From top to bottom, the trench width is $L_y = 7.93R_e$, $9.73R_e$, and $8.65R_e$, respectively. The sidewalls are A-selective.

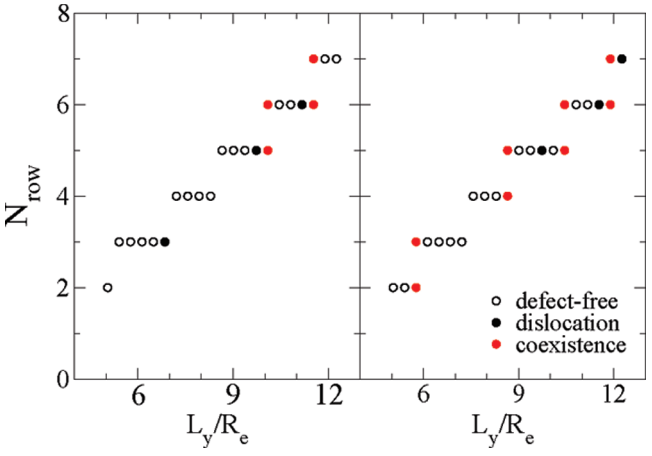

Figure 5. Number of rows of cylinders as a function of the trench width for a neutral trench (left) and a selective trench (right). The type of domain arrangement is indicated.

considered, yield perfect ordering. Overall, the selectivity of sidewalls does not seem to have a large influence, even

Table 1. Properties of Domains as a Function of the Row Number[a]

row	σ_y/R_e	R/R_e	γ
1	0.058	0.351	1.37
2	0.075	0.341	1.30
3	0.074	0.341	1.30
4	0.058	0.351	1.37

[a] The quantity σ_y denotes the standard deviation in the lateral position, R the domain radius, and γ the eccentricity ratio.

though coexistence arrangements appear more common in the selective trench.

When placed in a trench, the diblock cannot maintain its bulk properties. Confinement affects the lateral spacing between rows, as well as the longitudinal spacing of domains d_x, which denotes here the mean distance along the x-axis between two neighboring cylinders in the same row. For instance, in defect-free configurations where $N_{row} = 3$, the longitudinal spacing ranges from $d_x = 1.90R_e$ to $1.67R_e$, a significant deviation from the bulk spacing $d_0 = 1.74R_e$. The distortion of the hexagonal array has its origins in several factors. First, sidewalls modify domain properties in their vicinity, a boundary effect that will be dominating in the narrowest trenches. Second, the hexagonal array of domains, while remaining defect-free, deforms to accommodate the constraints imposed by the lateral confinement; this global distortion is seen in the largest trenches, where $d_x = 1.81R_e$ or $d_x = d_0$ depending on the width.

While Figure 5 provides a first characterization of commensurability effects, it does not give an estimate of defect density. For one test case, we now examine the statistical likelihood of obtaining a defect-free arrangement. Because strong confinement and wetting impose stronger constraints on the self-assembly, we choose a rather narrow trench, that can accommodate four rows, and whose sidewalls are selective. Also, in contrast to a neutral surface that experimentally requires a highly specific composition for the brush grafted on the wall (see ref 53, however), selective walls might apply to a broader range of experimental conditions. Large systems are used; they comprise more than 40 domains per row, and finite-size effects are small. Four distinct values of the trench width ($L_y = 7.39R_e$, $7.57R_e$, $7.75R_e$, and $7.93R_e$) are considered, with ten realizations in each case. As previously, all systems reach a stable state after 10^5 MCS. Only one trench width ($L_y = 7.57R_e$) yields a defect-free arrangement in all ten realizations, which corresponds to a total of 1800 cylinders. Other trenches lead to defects in two realizations out of 10, indicating that the "commensurability window" for this particular system is relatively narrow and spans less than $0.36R_e$, or about10 nm.

Focusing on the optimal width, we characterize the properties of individual domains. Features important for applications include the uniformity in domain size and row spacing, and the accuracy in placement along the row. Experiments with spheres have shown significant variations in domain size and row spacing across the trench,[16] whereas better uniformity was observed for cylinders.[15] Domain properties, computed in each of the four rows, are given in Table 1.[64] The two inner rows and two edge rows have rather similar properties. The domain radius and eccentricity ratio show little difference (3% and 5% variation, respectively) and the lateral spacings between rows are rather close ($0.403R_e$, $0.422R_e$, and $0.403R_e$). Finally, the placement error in the lateral position, i.e. the standard deviation in the y-coordinate, is smaller for the edge rows. Assuming $d_0 = 30$ nm as above yields $\sigma_y \simeq 2$ nm.

What remains to be examined is the longitudinal order, i.e., how domains are positioned along the rows. The first

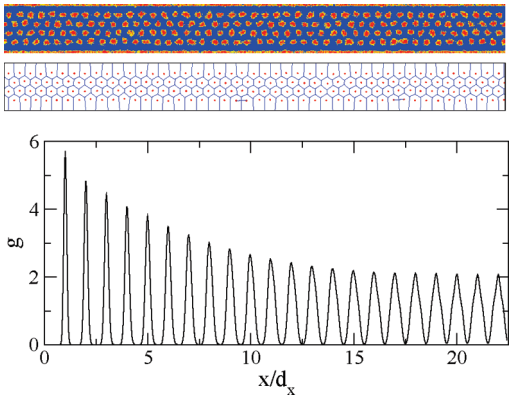

Figure 6. Pair correlation function for the longitudinal position of domains. The quantity d_x represents the mean distance between domains along the row. A representative configuration, and its Voronoi diagram, are shown above.

observation is that the ten realizations analyzed here are all defect-free, but they do not have the same number of domains per row. Indeed, eight realizations have 45 domains per row while the remaining two have 44 domains, yielding $d_x \simeq 1.777R_e$ and $d_x \simeq 1.818R_e$ respectively. This confirms that the confined diblock has a longitudinal spacing different from the nonconfined system.[65] Considering only the realizations with 45 domains per row, the pair correlation function for x-position can be computed; the correlation functions do not depend on the row considered and Figure 6 shows an average over the four rows. Upon increasing the distance between domains, the correlation peaks broaden, with a full width at half-maximum that increases from $0.1R_e$ to $0.2R_e$, but correlations remain high even at a distance of 20 domain spacings.

This section has identified a set of trench parameters that yield defect-free arrays with a high degree of reliability, and a tight distribution of placement error in lateral position. Addressable media requires, however, that the longitudinal position of each domain be specified with high accuracy. This requirement corresponds to a fixed number of domains per row, and implies that additional features must be used to locally pin the domains on a reference position. One can envision modulation in the trench width, protrusions along the trench walls, two-dimensional confinement or patterning the surface of the trench. With the system studied here, the spacing between such registration features should not exceed 40 domains, and should be smaller if high positioning accuracy is needed.

C. Chemical Patterns. In the patterns considered here, the patterned spots are circular with a radius $d_P/4$, and are arranged on a hexagonal array with spacing d_P. While the spots are always A-selective, the nonpatterned area, hereafter called "background", is either neutral or B-selective. For conciseness, those two patterns are called "neutral" (N) and "selective" (S). The third pattern is "incomplete" (I), with a neutral background and every other row removed, as shown in Figure 7.

We first investigate the tolerance of self-assembly against a small mismatch between the copolymer natural spacing and the pattern dimension. Considering only the pattern S, the pattern spacing d_P is changed systematically, from $1.6R_e$ to $1.95R_e$. At least five realizations, each containing $N_{spot} = 48$ patterned spots, are obtained for each pattern spacing. As shown in Figure 8, the number of domains N_{dom} increases with time until it reaches N_{spot}, at which point a vertical cylinder lays above every spot. For all pattern spacings $1.65 < d_P/R_e < 1.85$, a defect-free structure is reached ; outside this range, perfect ordering does not occur within the

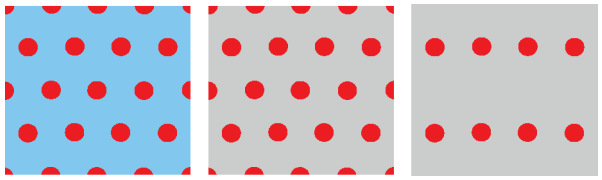

Figure 7. The three chemical patterns considered in this study: selective (S), neutral (N), and incomplete (I). The red spots attract the minority block (A beads); the blue background is selective to the majority block (B beads), whereas the gray background is neutral.

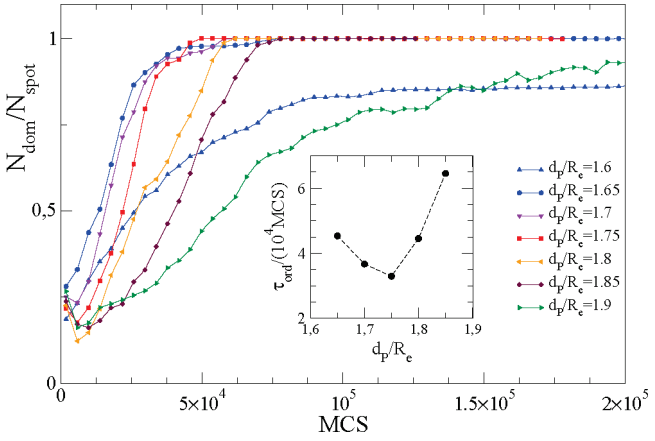

Figure 8. Influence of the chemical pattern spacing d_P on the self-assembly process. The number of domains N_{dom}, as seen from a top view, is shown as a function of time for d_P/R_e ranging from $1.6R_e$ to $1.9R_e$ ($d_0 = 1.74R_e$). N_{spot} is the number of patterned spots. (Inset) The quantity τ_{ord} is the time at which the system has reached a defect-free arrangement. The line is a guide to the eye.

accessible simulation time (2×10^5 MCS). Note that this estimate for the "tolerance window" might be affected by the finite-size of the system and the periodic boundary conditions.[66] The time necessary to reach perfect ordering depends strongly on d_P, as can be seen in the inset of Figure 8. Not surprisingly, faster ordering is observed for $d_P \simeq d_0$. On the other hand, for the same amount of deviation from d_0, the ordering observed with $d_P < d_0$ is faster than the ordering with $d_P > d_0$. A likely factor is that a smaller d_P corresponds to a lower number of chains in each domain (660 for $d_P = 1.65R_e$ against 830 for $d_P = 1.85R_e$), making it easier for the self-assembly to proceed.

The properties of domains in the defect-free structures are shown in Figure 9. The distance between nearest-neighbors d and the radius R exhibit Gaussian-like distributions; both quantities are dictated by the pattern spacing, with $d = d_P$ and R/d_P remaining close to 0.2. The width of the distribution shows little change upon increasing the pattern spacing; only the eccentricity ratio becomes slightly larger. Overall, a small mismatch between d_P and d_0 yields a change in spacing, but does not appear to perturb significantly domain properties.

Our observations can be compared to experimental results[41] obtained on a system whose parameters approximately match the case considered here.[67] Experiments show perfect ordering for $d_P = 1.06d_0$ and defects for $d_P = 0.92d_0$; these results are consistent with the tolerance window determined here. The properties of individual domains can also be determined by imaging the top free surface of the thin film with scanning electron microscopy. The distribution of domain size was found to be narrow with a ratio of the standard deviation to the mean radius of 0.046, slightly below our simulation result of 0.054. The mean eccentricity

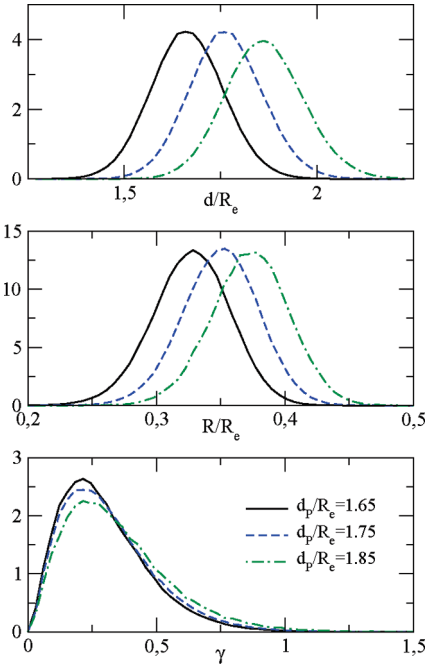

Figure 9. Properties of domains as seen from a top view, for self-assembly on the pattern S with spacings d_P/R_e. From top to bottom, the distance to nearest neighbors, the domain radius and the eccentricity ratio are shown. All curves are probability distributions.

of domains was in the range 0.48−0.55, in agreement with our value of 0.52−0.54.

Fixing the pattern spacing d_P to $1.75R_e$, we now change the type of pattern by considering the neutral (N) and incomplete (I) patterns. The system size and number of realizations are the same as previously. All systems yield defect-free self-assembly. The top section of domains have the same properties: all distribution curves fall closely on one another, as shown in Figure 10. Interestingly, the interpolation of cylinders on incomplete patterns does not induce any changes in those properties, at least from a top-view characterization.

The ideal patterns considered so far are approximations of the real patterns used in experiments. Indeed, the noise inherent in the patterning process gives rise to imperfections in the size and position of the spots. We now investigate the influence of this noise on the self-assembled structure, considering noise only in position. Each spot is displaced away from its ideal position by a vector $\Delta\mathbf{r}$, whose coordinates Δx and Δy are randomly chosen in the interval $[-\sigma_P; \sigma_P]$.[68] For the three patterns S, N, and I, and noise strength $\sigma_P/R_e = 0.2, 0.3, 0.4, 0.5$, three realizations, each containing 120 spots, were simulated. For the strongest noise, none of the systems formed a periodic array within the time considered (2×10^5 MCS). On the other hand, for $\sigma_P/R_e = 0.4$ or less, defect-free structures are obtained with all three patterns. The ordering time τ_{ord} depends strongly on the pattern type and noise strength, as can be seen in Table 2. On the pattern S, τ_{ord} shows a 5-fold increase upon varying σ from $0.2R_e$ to $0.4R_e$. The increase is not as pronounced for the two other patterns. As a result, at low noise, self-assembly is faster on the pattern S, while at high noise, it is slower than self-assembly on patterns N and I. Note that a selective background exerts a stronger effect of the chain arrangement since both the minority and majority blocks are constrained to their preferred area (spot and background respectively). On the other hand, a neutral background leaves more flexibility to the system, which can then accommodate more easily the noise-induced perturbation.

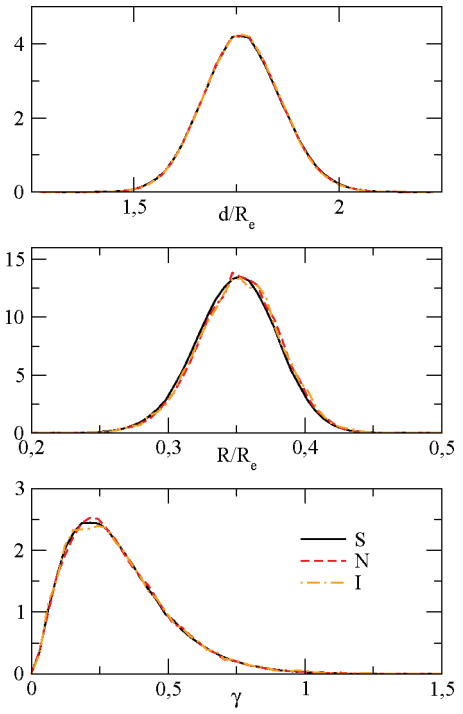

Figure 10. Properties of domains as seen from a top view, for self-assembly on the patterns S, N, and I. From top to bottom, the distance to nearest neighbors, the domain radius and the eccentricity ratio are shown. All curves are probability distributions.

Table 2. Average Ordering Time τ_{ord} Necessary To Reach Defect-Free Self-Assembly as a Function of Pattern Noise σ_P, on Three Different Chemical Patterns[a]

σ_P/R_e	selective	neutral	incomplete
0.2	22	29	37
0.3	41	41	56
0.4	107	66	83
0.5	> 200	> 200	> 200

[a] τ_{ord} is given in units of 10^3 MCS.

While the top views of the self-assembled systems indicate perfect ordering, the shape and properties of the domains below the surface remain to be characterized. Cross-sectional properties are particularly challenging to obtain in experiments, as they involve visualizing cross sections of extremely thin film. To determine the three-dimensional shape of the domains in our simulations, cross sections were taken at various heights. Because they are obtained from a long time average (10^3 MCS), those cross sections characterize the average perturbation in domain position induced by the pattern noise rather than the instantaneous variations in shape or position.

The cross sections shown in Figure 11 illustrate the rectification effect. While the patterned spots dictate the domain positions in the vicinity of the substrate, the induced deviations decrease as one moves away from the substrate. At half-height ($z \simeq 1.25R_e$), domains have recovered a very good regularity in position. Since for the noise $\sigma_P = 0.4R_e$, the hexagonal arrangement of spots appears to be lost, it is remarkable that such patterns can still allow defect-free self-assembly. However, with the pattern average spacing almost exactly that of the block copolymer, and the spot position still far from random, a defect-free array of cylindrical domains remains the preferred state of the block copolymer. Rectification also occurs on incomplete patterns. In the vicinity of the substrate, two groups of domains are clearly

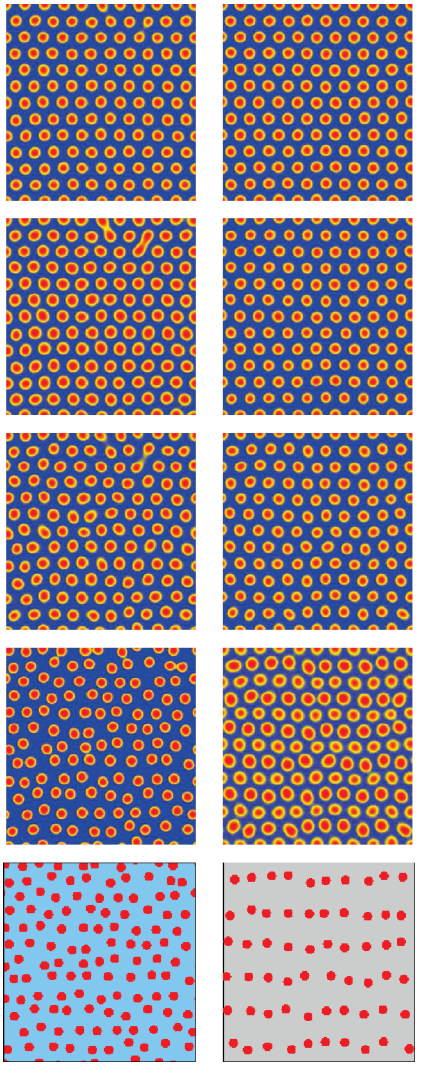

Figure 11. Rectification effect for a block copolymer self-assembled on a chemical pattern with noise in the position of the patterned spots. Each color map shows the local composition in a horizontal cross-section of the thin film, taken at a height $z = 0.15$, 0.45, 0.85, and 1.25 R_e, from bottom to top. The thickness of the films is $2.2R_e$. The pattern is selective (left) or incomplete (right) and is shown below. The noise in spot position is $\sigma_P = 0.4R_e$ in both cases.

visible: the noninterpolated cylinders, which lay above a spot, and the interpolated cylinders, which lay above the neutral background. At half-height, the two groups are undistinguishable.

Figure 12 provides a quantitative measure of the rectification within the film. To evaluate the placement error in domain position, we computed as a function of height the root-mean-square distance between the domain center and its ideal position (i.e., the position of the spot center in the absence of noise). Each curve $\sigma(z)$ shown in Figure 12 represents an average over hundreds of cylinders. A common behavior is observed for all patterns and noise levels considered. Each curve $\sigma(z)$ starts from its maximum value at the substrate, then shows a marked decrease, reaches a local minimum around midheight, and finally increases slightly at the top surface. On the other hand, the type of pattern influences the extent of rectification. On pattern S, the placement error at the top surface is independent of the noise strength. On pattern I, the effect of noise propagates all the way to the top surface, and the deviation $\sigma(z)$ in the upper half of the film increases with the strength of the noise.

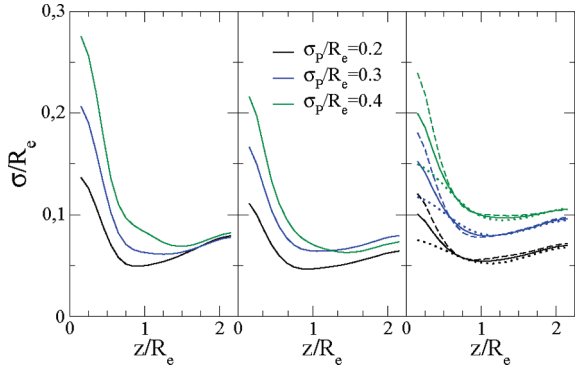

Figure 12. Rectification effect within the film on chemical patterns S, N, and I (from left to right). The strength of noise in spot position is σ_P/R_e = 0.2, 0.3, or 0.4. $\sigma(z)$ is the mean square distance between the domain center at height z and its ideal position, averaged over all domains. For pattern I (right), curves for the interpolated domains and noninterpolated domains are also shown, with dotted and dashed lines, respectively.

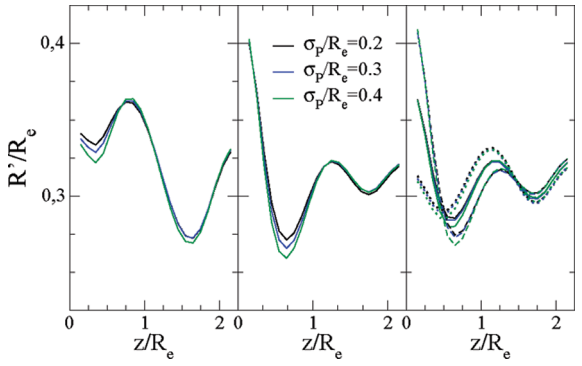

Figure 13. Average domain radius as a function of height in the film, for self-assembly on chemical patterns S, N, and I (from left to right). The strength of noise in spot position is σ_P/R_e = 0.2, 0.3, or 0.4. For the pattern I, curves for the interpolated domains and noninterpolated domains are also shown, with dotted and dashed lines, respectively.

Note, however, that the position of interpolated cylinders is not constrained by the substrate and is much closer to that of an ideal placement.

For all systems studied here, the decay in placement error is complete at a distance of approximately $1R_e$ from the substrate. While this value is almost independent of strength noise, it probably depends on the block copolymer film, and film thickness, as suggested in ref 54. The system considered in that particular study corresponded to lamellae-forming block copolymers on a striped patterned surface, and the pattern imperfection consisted of undulations in the line egde. Single-chain in mean field simulations and phenomenological theory showed that the characteristic length for the decay of substrate-induced roughness depends on the undulation wavelength, but also on the diblock natural spacing, and film thickness. This conclusion is likely to be valid for the case considered here, even though the pattern imperfection is random rather than periodic.

As can be seen in Figure 12, the area of domains is not constant throughout the thickness of the film, implying that the domains are not, strictly speaking, cylinders. The domain size is estimated by computing the radius R', which results from an average over time and all domains. Figure 13 shows how R' varies across the film thickness. Surprisingly, the curves are independent of the noise level; they depend only on the type of pattern. In the vicinity of the substrate, the domain size depends on the type of background. A neutral background allows a maximal number of minority blocks to be located near the patterned spot, whereas the selective background limits this tendency. As a result, $R'(z \simeq 0)$ is significantly larger for a neutral background. Between the bottom and the top surface, all $R'(z)$ curves show pronounced oscillations, with a domain area that can vary by a factor of 2. Depending on the technique used (e.g., by etching), the observations above could have implications for the transfer of the self-assembled domains into a specific nanostructure.

IV. Conclusion

We have examined the ability of two prototypical patterns to generate defect-free arrays of vertical cylinders: a trench and a substrate chemically patterned with spots. For the trench, a set of parameters was identified that consistently yields defect-free structures and good uniformity of domain properties across the trench. With ten realizations, each containing almost two hundred cylinders, the simulated systems comprise almost 2000 domains self-assembled without a single defect, suggesting an upper bound of 10^{-3} for the defect density. However, if a parallel-sided trench can ensure lateral ordering, the longitudinal order of domains requires additional features. For the system studied here, the repeat spacing of those features should not exceed 40 domains. Chemically patterned substrates were found to yield perfect ordering and registration over a broad range of conditions. The observation most relevant to technological applications is the interplay between the rectification and interpolation effects. For the particular system studied here, we find that noise-induced perturbations of the domains decay almost completely over a distance $1R_e$. Although the influence of noise is still detectable at the top surface, self-assembly on incomplete patterns with a multiplication factor of 2 yields a significant improvement in placement error of domains.

We have relied on a pseudodynamics generated by Monte Carlo simulations with local moves, and focused on the stable configurations obtained at long times. While the defect-free arrangements presumably correspond to equilibrium, it remains to be shown whether defective configurations are kinetically trapped metastables states and how such trapping occurs. Because each domain involves on the order of 10^3 chains, Monte Carlo moves that remain at the single chain level can not be expected to yield global equilibration in domain arrangement. Collective moves that modify entire domains would be required. Alternatively, thermodynamic integration[37,55] could be used to compute the free energy difference between two distinct morphologies, but all possible arrangements would then have to be identified. Another approach might rely on controlled temperature annealing, rather than a quench from the disordered phase. Annealing should avoid being trapped in (at least some) metastable states, and might extend the commensurability or tolerance windows, as was observed for confined blends.[33]

The model and the Monte Carlo method used here enable the simulation of hundreds of domains, in three-dimensional systems, on single processor machines. Yet, straightforward improvements could be made, first and foremost, using a more realistic dynamics. While the grid-based implementation employed here is very efficient, devising a genuine dynamics is difficult because forces between beads are ill-defined. This limitation can be lifted by using a gridless implementation,[56] which, at the cost of longer computation time, allows one to use Langevin or Brownian dynamics. Furthermore, force-based dynamics are amenable to easy parallelization, leading to gains of at least an order of magnitude in system size. This would facilitate prediction of defect densities as low as 10^{-4} or 10^{-5}, i.e., figures in the realm of defect densities envisioned for real applications.

Acknowledgment. This work was supported by the National Science Foundation (NSF) through the University of Wisconsin Nanoscale Science and Engineering Center (NSEC), by the Semiconductor Research Corporation (SRC), and by the National Institute for Nano-Engineering (NINE) at Sandia National Laboratories. J.J.d.P. is grateful for a Marie Curie Fellowship from the European Community.

References and Notes

(1) Hamley, I. *The Physics of Block Copolymers*; Oxford University Press: Oxford, U.K., 1998.
(2) Abetz, V.; Simon, P. F. W. *Block Copolymers I*; Advances in Polymer Science 189; Springer-Verlag: Berlin, 2005; p 125.
(3) Lazzari, M.; Liu, G.; , Lecommandoux, S., Eds. *Block Copolymers in Nanoscience*; Wiley: New York, 2003.
(4) Harrison, C.; Cheng, Z.; Sethuraman, S.; Huse, D. A.; Chaikin, P. M.; Vega, D. A.; Sebastian, J. M.; Register, R. A.; Adamson, D. H. *Phys. Rev. E* **2002**, *66*, 011706.
(5) Harrison, C.; Angelescu, D. E.; Trawick, M.; Cheng, Z.; Huse, D. A.; Chaikin, P. M.; Vega, D. A.; Sebastian, J. M.; Register, R. A.; Adamson, D. H. *Europhys. Lett.* **2004**, *67*, 800.
(6) Vega, D. A.; Harrison, C. K.; Angelescu, D. E.; Trawick, M. L.; Huse, D. A.; Chaikin, P. M.; Register, R. A. *Phys. Rev. E* **2005**, *71*.
(7) Kramer, E. *Nature* **2005**, *437*, 824.
(8) Cheng, J.; Ross, C.; Smith, H.; Thomas, E. *Adv. Mater.* **2006**, *18*, 2505.
(9) Cheolmin, P.; Jongseung, Y.; Edwin L., T. *Polymer* **2003**, *44*, 6725.
(10) Segalman, R. A. *Mater. Sci. Eng.: R: Rep.* **2005**, *48*, 191.
(11) Segalman, R. A.; Yokoyama, H.; Kramer, E. J. *Adv. Mater.* **2001**, *13*, 1152.
(12) Ruiz, R.; Sandstrom, R. L.; Black, C. T. *Adv. Mater.* **2007**, *19*, 587.
(13) Park, S. M.; Stoykovich, M. P.; Ruiz, R.; Zhang, Y.; Black, C. T.; Nealey, P. E. *Adv. Mater.* **2007**, *19*, 607.
(14) Sundrani, D.; Darling, S. B.; Sibener, S. J. *Nano Lett.* **2004**, *4*, 273.
(15) Xiao, S.; Yang, X.; Edwards, E. W.; La, Y.-H.; Nealey, P. F. *Nanotechnology* **2005**, *16*, S324.
(16) Cheng, J. Y.; Ross, C. A.; Thomas, E. L.; Smith, H. I.; Vancso, G. J. *Adv. Mater.* **2003**, *15*, 1599.
(17) Ruiz, R.; Ruiz, N.; Zhang, Y.; Sandstrom, R. L.; Black, C. T. *Adv. Mater.* **2007**, *19*, 2157.
(18) Cheng, J. Y.; Mayes, A. M.; Ross, C. A. *Nat. Mater.* **2004**, *3*, 823.
(19) Cheng, J. Y.; Zhang, F.; Smith, H. I.; Vancso, G. J.; Ross, C. A. *Adv. Mater.* **2006**, *18*, 597.
(20) Chuang, V. P.; Cheng, J. Y.; Savas, T. A.; Ross, C. A. *Nano Lett.* **2006**, *6*, 2332.
(21) Bita, I.; Yang, J.; Jung, Y.; Ross, C.; Thomas, E.; Berggren, K. *Science* **2008**, *321*, 939.
(22) Park, S.; Lee, D. H.; Xu, J.; Kim, B.; Hong, S. W.; Jeong, U.; Xu, T.; Russell, T. P. *Science* **2009**, *323*, 1030.
(23) Kim, S. O.; Solak, H. H.; Stoykovich, M. P.; Ferrier, N. J.; de Pablo, J. J.; Nealey, P. F. *Nature* **2003**, *424*, 411.
(24) Stoykovich, M. P.; Müller, M.; Kim, S. O.; Solak, H. H.; Edwards, E. W.; de Pablo, J. J.; Nealey, P. F. *Science* **2005**, *308*, 1442.
(25) Ruiz, R.; Kang, H.; Detcheverry, F. A.; Dobisz, E.; Kercher, D. S.; Albrecht, T. R.; de Pablo, J. J.; Nealey, P. F. *Science* **2008**, *321*, 936.
(26) Cheng, J. Y.; Rettner, C. T.; Sanders, D. P.; Kim, H.-C.; Hinsberg, W. D. *Adv. Mater.* **2008**, *20*, 3155.
(27) Tada, Y.; Akasaka, S.; Yoshida, H.; Hasegawa, H.; Dobisz, E.; Kercher, D.; Takenaka, M. *Macromolecules* **2008**, *41*, 9267.
(28) Chen, H.; Chakrabarti, A. *J. Chem. Phys.* **1998**, *108*, 6897.
(29) Wu, X.-F.; Dzenis, Y. A. *J. Chem. Phys.* **2006**, *125*, 174707.
(30) Hur, S.-M.; Garcia-Cervera, C. J.; Kramer, E. J.; Fredrickson, G. H. *Macromolecules* **2009**, *42*, 5861.
(31) Stoykovich, M. P.; Kang, H.; Daoulas, K. C.; Liu, G.; Liu, C.-C.; de Pablo, J. J.; Müller, M.; Nealey, P. F. *ACS Nano* **2007**, *1*, 168.
(32) Petera, D.; Muthukumar, M. *J. Chem. Phys.* **1998**, *109*, 5101.
(33) Bosse, A. W.; Garcia-Cervera, C. J.; Fredrickson, G. H. *Macromolecules* **2007**, *40*, 9570.
(34) Fredrickson, G. H., *The Equilibrium Theory of Inhomogeneous Polymers*; Clarendon Press: Oxford, U.K., 2006.
(35) Detcheverry, F. A.; Kang, H.; Daoulas, K. C.; Müller, M.; Nealey, P. F.; de Pablo, J. J. *Macromolecules* **2008**, *41*, 4989.
(36) Detcheverry, F. A.; Pike, D. Q.; Nagpal, U.; Nealey, P. F.; de Pablo, J. J. *Soft Matter* **2009**, *5*, 4858.
(37) Detcheverry, F. A.; Liu, G.; Nealey, P.; de Pablo, J. J. *Macromolecules* **2010**, *43*, 3446.
(38) Müller, M.; Daoulas, K. C. *J. Chem. Phys.* **2008**, *129*, 164906.
(39) Fredrickson, G. H.; Ganesan, V.; Drolet, F. *Macromolecules* **2002**, *35*, 16.
(40) Müller, M.; Schmid, F. *Advanced Computer Simulation Approaches for Soft Matter Sciences*; Advances in Polymer Science 185; Springer-Verlag: Berlin and Heidelberg, Germany, 2005; p 1.
(41) Park, S.-M.; Craig, G. S. W.; Liu, C.-C.; La, Y.-H.; Ferrier, N. J.; Nealey, P. F. *Macromolecules* **2008**, *41*, 9118.
(42) Pike, D. Q.; Detcheverry, F. A.; Müller, M.; de Pablo, J. J. *J. Chem. Phys.* **2009**, *131*, 084903.
(43) Daoulas, K. C.; Muller, M.; Stoykovich, M. P.; Park, S. M.; Papakonstantopoulos, Y. J.; de Pablo, J. J.; Nealey, P. F.; Solak, H. H. *Phys. Rev. Lett.* **2006**, *96*, 036104.
(44) Suh, K. Y.; Kim, Y. S.; Lee, H. H. *J. Chem. Phys.* **1998**, *108*, 1253.
(45) Huinink, H. P.; Brokken-Zijp, J. C. M.; van Dijk, M. A.; Sevink, G. J. A. *J. Chem. Phys.* **2000**, *112*, 2452.
(46) Wang, Q.; Nealey, P. F.; de Pablo, J. J. *Macromolecules* **2001**, *34*, 3458.
(47) Yang, Y.; Qiu, F.; Zhang, H.; Yang, Y. *Polymer* **2006**, *47*, 2205.
(48) Heckmann, M.; Drossel, B. *Macromolecules* **2008**, *41*, 7679.
(49) Meng, D.; Wang, Q. *J. Chem. Phys.* **2007**, *126*, 234902.
(50) Mattioni, L.; Wittmer, J.; Baschnagel, J.; Barrat, J.; Luijten, E. *Eur. Phys. J. E* **2003**, *10*, 369.
(51) Fetters, L.; Lohse, D.; Richter, D.; Witten, T.; Zirkel, A. *Macromolecules* **1994**, *27*, 4639.
(52) Sundrani, D.; Darling, S. B.; Sibener, S. J. *Langmuir* **2004**, *20*, 5091.
(53) Han, E.; Stuen, K. O.; La, Y.-H.; Nealey, P. F.; Gopalan, P. *Macromolecules* **2008**, *41*, 9090.
(54) Daoulas, K. C.; Mueller, M.; Stoykovich, M. P.; Kang, H.; de Pablo, J. J.; Nealey, P. F. *Langmuir* **2008**, *24*, 1284.
(55) Müller, M.; Daoulas, K. C. *J. Chem. Phys.* **2008**, *128*, 024903.
(56) Detcheverry, F. A.; Pike, D. Q.; Nealey, P. F.; Müller, M.; de Pablo, J. J. *Phys. Rev. Lett.* **2009**, *102*, 197801.
(57) If not mentioned otherwise, boundary conditions in the other directions are periodic.
(58) For the film thickness $L_z = 2.2R_e$ used throughout the work, simulation of a very large system (236 vertical cylinders) confirms the morphology observed with the smaller system size.
(59) Note that each individual domain involves more than 700 chains.
(60) The maximal displacement in each direction is 0.75 b, where $b^2 = R_e^2/(\mathrm{N}-1)$ is the mean square bond length.
(61) The distribution of ϕ is bimodal with a minimum at zero.
(62) The occurrence of two bridges connecting three clusters together is rare and is neglected here.
(63) The term coexistence as used here does not imply a phase coexistence between two phases of equal free energy.
(64) Domain properties are computed over a time span of 20000 MCS that starts after the defect-free configuration is reached, and are subsequently averaged over ten realizations. Gaussian-like distributions are found for the domain size and lateral position, which can therefore be characterized according to their average value and standard deviation.
(65) The trench length is almost perfectly commensurate with d_0, since $80/46 = 1.739 \simeq d_0$, implying that a d_0 spacing is not prevented by the finite-size of the trench.
(66) The simulation box accommodates 48 cylinders, a rather large number, but artificially inhibits defects that could arise in larger boxes.
(67) The diblock is a PS-PMMA polymer with molecular weight 50 + 20 kg.mol^{-1}, that approximately corresponds to $\sqrt{N} = 90$, somewhat below the value $\sqrt{N} = 128$ employed here. The film thickness is $L_z/d_0 = 1.24$ in experiments, whereas $L_z/d_0 = 1.26$ in simulations; $\chi N = 25$ in both cases.
(68) We chose a bounded distribution for the displacement probability because with Gaussian or other nonbounded distributions, large deviations are allowed and the overlap between spots yields a high probability of defects.